

Turbulent flow over a dune: Green River, Colorado

Jeremy G. Venditti¹* and Bernard O. Bauer²

¹ Department of Geography, University of British Columbia, Vancouver, British Columbia, V6T 1Z2, Canada

² Department of Geography, University of Southern California, Los Angeles, CA 90089-0255, USA

*Correspondence to:

J. G. Venditti, Department of
Earth and Planetary Sciences,
University of California, 307
McCone Hall, Berkeley,
CA 94720, USA.
E-mail: jgvenditti@yahoo.ca

Abstract

Detailed echo-sounder and acoustic Doppler velocimeter measurements are used to assess the temporal and spatial structure of turbulent flow over a mobile dune in a wide, low-gradient, alluvial reach of the Green River. Based on the geometric position of the sensor over the bedforms, measurements were taken in the wake, in transitional flow at the bedform crest, and in the internal boundary layer. Spatial distributions of Reynolds shear stress, turbulent kinetic energy, turbulence intensity, and correlation coefficient are qualitatively consistent with those over fixed, two-dimensional bedforms in laboratory flows. Spectral and cospectral analysis demonstrates that energy levels in the lee of the crest (i.e. wake) are two to four times greater than over the crest itself, with minima over the stoss slope (within the developing internal boundary layer). The frequency structure in the wake is sharply defined with single, dominant peaks. Peak and total spectral and cross-spectral energies vary over the bedform in a manner consistent with wave-like perturbations that 'break' or 'roll up' into vortices that amalgamate, grow in size, and eventually diffuse as they are advected downstream. Fluid oscillations in the lee of the dune demonstrate Strouhal similarity between laboratory and field environments, and correspondence between the peak frequencies of these oscillations and the periodicity of surface boils was observed in the field. Copyright © 2005 John Wiley & Sons, Ltd.

Keywords: fluvial bedforms; dunes; spectral analysis; turbulence; Strouhal number

Received 26 November 2002;
Revised 15 March 2004;
Accepted 20 April 2004

Introduction

Alluvial river channels are the manifestation of a suite of hydraulic and sedimentary processes acting within the channel and catchment area. These processes act to modify and adjust the channel system at spatial and temporal scales ranging from those of individual particle movements to ones of meander-bend migration and floodplain evolution. Our ability to understand and predict fluvial processes across this range of scales remains rudimentary because of the complex nature of the interaction of fluids and sediments under the constraint of varying boundary conditions (McLean *et al.*, 1996). In sand-bedded alluvial channels, the bottom boundary consists of a mobile bed comprising bedforms of many different scales and geometries. A deeper knowledge of how fluvial dunes interact with the flow field is crucial to understanding sediment transport processes in rivers, resistance to flow, and ultimately, to understanding the evolution of alluvial systems.

Fluid flows over two-dimensional laboratory dunes and negative steps have been studied extensively, and several major components are commonly recognized in the flow field (Figure 1). Typically, there is an outer region that is not directly influenced by the detailed geometry of the bedforms insofar as the flow responds largely to the spatially averaged resistance effect communicated to it from below. Between the outer region and the mobile sediment bottom are several intervening zones whose dynamics differ from classic turbulent boundary layer flows over flat beds. In particular, the presence of a dune leads to significant form drag due to asymmetries in the flow field over the upstream (stoss) and downstream (lee) sections of the dune. As the flow moves up the gently sloping stoss side of the dune, the streamlines converge and the fluid is accelerated toward a maximum depth-averaged velocity near the crest. At the brink point between the stoss and lee, the streamlines detach from the surface, leading to flow separation in the lee of the dune. Provided that the lee side slope is sufficiently steep, a distinct separation cell or recirculation 'bubble' occupies the near-bottom region immediately downstream of the dune crest. Flow in the separation cell can be quite variable, but in a time-averaged sense there exists a counter-rotating eddy with upstream velocity along the bottom. At

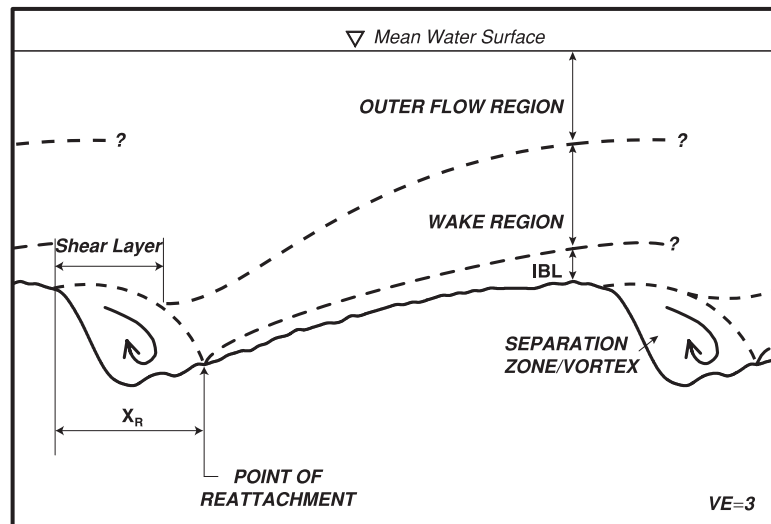


Figure 1. Schematic of boundary layer structure over a dune (based on McLean, 1990, reproduced by permission of Elsevier). X_R is horizontal distance from the crest to the reattachment point and IBL is an abbreviation for internal boundary layer.

the downstream margin of the cell, the separated flow reattaches to the bottom at a downstream distance, X_R , that is on average $5H$, where H is the crest height (Engel, 1981). The reattached flow accelerates up the stoss side of the dune, and an accompanying internal boundary layer (IBL) grows in thickness from the point of reattachment toward the dune crest. The character of the IBL is related to skin friction imparted by grain roughness, although disturbance by eddies from the wake region can be frequent (Nelson *et al.*, 1993). Small ripples migrating up the stoss slope of dunes further complicate the structure of the IBL.

The near-bottom flow region, composed of the separation cell and IBL, is linked to the outer flow region through the intervening wake region and shear layer. The dynamics of these latter two flow features are relatively poorly understood, even though they have generated considerable interest because of ramifications for sediment transport, the stability of bedforms, and the existence of quasi-coherent flow structures (McLean, 1990; Nelson *et al.*, 1993; McLean *et al.*, 1994; Bennett and Best, 1995; Venditti and Bennett, 2000). For example, the origin of kolks and boils in large fluvial systems (e.g. Matthes, 1947), which are typically heavily sediment-laden, has been variously ascribed to the boundary-layer bursting process (Jackson, 1976; Yalin, 1992), Kelvin–Helmholtz instabilities on the shear layer (Kostaschuk and Church, 1993; Bennett and Best, 1995; Venditti and Bennett, 2000), shear-layer destabilization coupled with ejection of slow-moving fluid from the recirculation bubble (Nezu and Nakagawa, 1993) and vortex shedding and amalgamation (Müller and Gyr, 1986). Most authors now acknowledge some interplay amongst the latter three processes (see discussion in Nezu and Nakagawa, 1993).

Much of what is understood about the flow structure over dunes has been learned in the controlled environment of laboratory flumes and few data sets have been collected over dunes in natural river channels. Field investigations include the work of Sukhodolov *et al.* (1998) who examined the turbulence properties of vertical profiles at a single channel cross-section. These measurements were not closely tied to bedforms in the channel; however, the work of Kostaschuk and collaborators in the Fraser River Estuary (see Kostaschuk, 2000; Kostaschuk and Church, 1993; Kostaschuk and Villard, 1996) is noteworthy in that the data sets are closely linked to the bedforms. However, the dunes differ from classic conceptions of fluvial bedforms because their development and morphology are influenced by tides in the channel.

The purpose of this paper is (1) to examine a set of field observations of flow over a dune formed under unidirectional flow conditions, and (2) to compare our measurements with detailed laboratory studies over dune in laboratory settings. The data set consists of high-frequency velocity and echo-sounder measurements taken above the stoss slope, crest, and trough of a migrating dune as it passed through a fixed instrument array deployed in a river. The data set is unique because the velocity measurement locations can be directly linked to the bedform. The time-averaged turbulence quantities are examined in the context of recent laboratory experiments that elucidate the detailed two-dimensional flow field over fixed bedforms (e.g. McLean, 1990; Nelson *et al.*, 1993; McLean *et al.*, 1994; Bennett and Best, 1995; Venditti and Bennett, 2000). Spectral and cospectral analyses are used to provide insight into the nature of oscillations embedded in the flow field at various points along the dune profile.

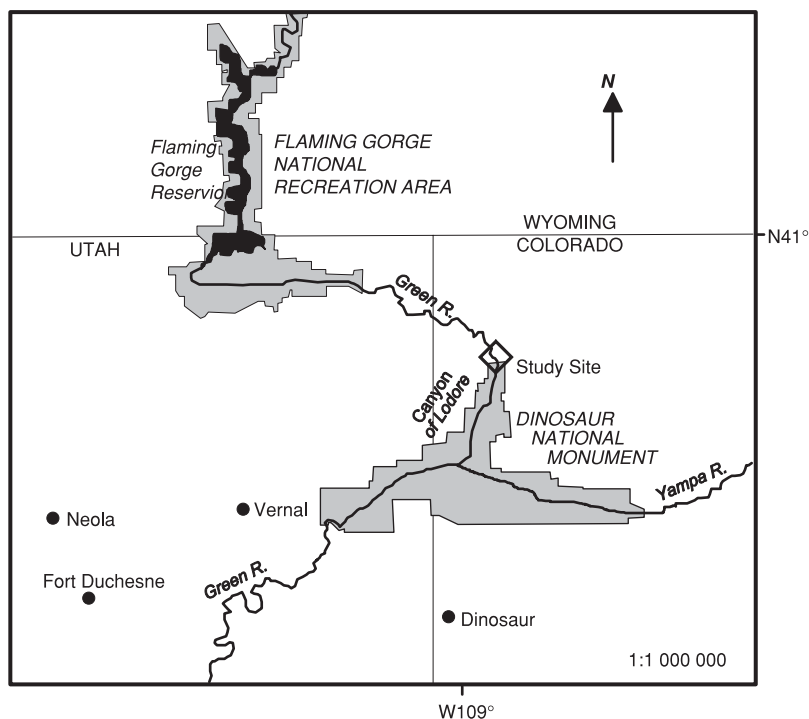


Figure 2. Study site location.

Methods

Field site

Field experiments were conducted in a low-sinuosity reach of the Green River approximately 1 km upstream from the Canyon of Lodore, Dinosaur National Monument, Colorado (Figure 2). Flow through this sand-bedded, alluvial reach is controlled by operations at Flaming Gorge Dam located 50 km upstream of the site. During the experiments, the discharge release from the dam was steady at $128 \pm 8 \text{ m}^3 \text{ s}^{-1}$ (4500 ± 300 cubic feet per second). There are no major tributaries between the dam and study site, although there are two small tributaries, Red Creek and Vermillion Creek, that contribute negligibly to main-stem discharge. Stage measurements remained constant throughout the measurement period, reaffirming the constant discharge regime.

As part of a larger project conducted for the National Park Service, repeat stream-gauging surveys were taken, and the reach-averaged summary data are presented in Table I. Sediment transport through the channel was bed load dominated with bed-material sizes in the coarse sand range ($D_{50} = 0.6 \text{ mm}$). The majority of sediment transport through the reach ($c. 1000 \text{ kg min}^{-1}$) was associated with the migration of bedforms. During storm events and flash floods, Red and Vermillion Creeks are capable of contributing large amounts of fine silt and clay that move through the system as wash load. During the experiments, these tributaries were not in flood and no wash load was observed. Suspended sediment concentrations (measured with an optical sensor) were negligible throughout the entire reach. With the exception of the gravel-bedded thalweg, sandy dunes occupied the channel bottom with $H = 0.2\text{--}0.4 \text{ m}$ and $\lambda = 4\text{--}5 \text{ m}$, where λ is dune wavelength.

The detailed flow data reported herein were collected during a 5.5-hour period on 3 June 1996 at the upstream end of an expansive low-amplitude channel bar. During this period, a two-dimensional dune with superimposed ripples migrated through the fixed instrument array.

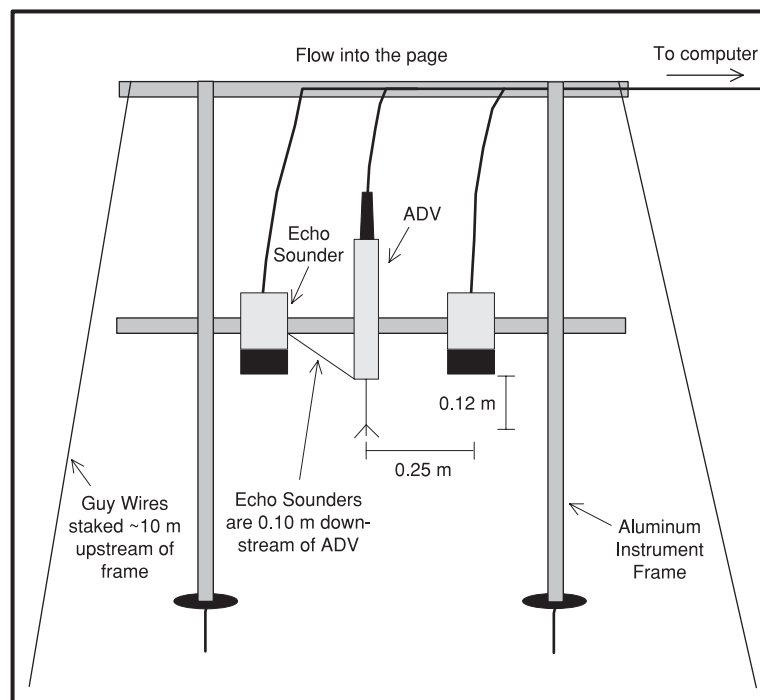
Instrument deployment and data processing

Topographic and hydraulic parameters were monitored using an array of sensors mounted on an aluminium frame. The frame was installed perpendicular to the mean surface flow lines and secured with guy wires, staked $c. 10 \text{ m}$ upstream and angled away from the frame (Figure 3). Instrument cables were run directly to a laptop computer-based data acquisition

Table I. Summary of total or average channel characteristics, Green River, upstream of Canyon of Lodore

Channel characteristic	Value
Slope, S	6.5×10^{-4} *
Mean depth, d_c (m)	1.5*
Discharge, Q ($\text{m}^3 \text{s}^{-1}$)	128
Channel width, b (m)	122
Mean flow velocity, $U_c = Q/bd_c$ (m s^{-1})	0.70
Bed shear stress, $\tau_o = \rho g d_c S$ (Pa)	9.56
Shear velocity, $u = \sqrt{\tau_o/\rho}$ (m s^{-1})	0.10
Darcy-Weisbach friction factor, $ff = 8\tau_o/\rho U_c^2$	0.16
Froude number, $Fr = U_c/\sqrt{gd_c}$	0.18
Reynolds number, $Re = U_c d_c/\nu$	8.1×10^5
Mean dune height, H (m)	c. 0.2–0.4
Mean dune wavelength, λ (m)	c. 4–5
Height–wavelength ratio, H/λ	0.04–0.10
Height–depth ratio, H/d	0.13–0.27
Bed load transport rate (kg min^{-1})	c. 1000*

* Provided by M. Kammerer, Department of Geography, University of Southern California.

**Figure 3.** Schematic of instrument frame.

system powered by batteries and a portable generator. A pontoon boat positioned downstream of the instrument array and held stationary by a spud-mount pole system (Stone and Morgan, 1992) served as a working platform.

Measurements of dune geometry were obtained using two echo sounders mounted 0.5 m apart (Figure 3). These units emit an acoustic signal at a frequency of 200 kHz and a pulse length of 250 μs with a nominal beam width of 10°. The acoustic signal is directed toward a solid boundary and the return signal is sensed, timed, and converted to an analogue voltage in proportion to the separation distance (depth). Minimum operating depth is 0.5 m and vertical resolution is 0.01 m (Mesotech, 1984). The echo sounder signals were sampled at a rate of 4 Hz. Examination of the

echo sounder time series showed only minor acoustic contamination, which was removed by a computer algorithm that discarded inordinately extreme values.

Fluid velocity was measured with an acoustic Doppler velocimeter (ADV) mounted between the echo sounders but displaced 0.10 m upstream to minimize flow interference (Figure 3). The ADV consists of a 0.3 m long probe fitted with an acoustic transmitter and three acoustic receivers. The transmitter sends an acoustic beam that is scattered by suspended particles in the sampling volume. The receivers sense the strength of the reflected signal as well as the Doppler shift caused by particles passing through the sensing volume, and these are used to estimate the three-dimensional velocity field at a point below the probe. The ADV measures instantaneous streamwise (u), spanwise (v), and vertical (w) velocities with a reported precision of $\pm 0.01 \text{ cm s}^{-1}$. The sampling volume is 1 cm^3 and it is focused 0.0528 m below the transmitter (Sontek, 1996). Flow velocity was recorded at the maximum sampling rate of 25 Hz for periods of 17 minutes at regular intervals (approximately every 0.5 hour) during the study period. A total of eleven files were collected spanning a 5.5 h period.

ADV signals are affected by Doppler (white) noise associated with the measurement process (Lohrmann *et al.*, 1994). The presence of this noise at high frequencies may create an aliasing effect from frequencies greater than the Nyquist frequency (herein $f_n = 12.5 \text{ Hz}$) that are folded into the lower frequencies. To remove possible aliasing effects, a recursive low pass filter with a half-power frequency of 5 Hz was applied to the time series. This filter effectively removes all variance at frequencies above f_n (e.g. Biron *et al.*, 1995). It is commonly accepted that turbulence spectra should exhibit a $-5/3$ roll off at high frequencies. Examination of the velocity spectra revealed that the spectra agree with this model up to $c. 4 \text{ Hz}$, where the slope changes (Figure 4a). Thus, the data were decimated to 4 Hz in order to ensure that the information in the time series above 4 Hz was removed. Only the information corresponding to the coarse-scale flow structures was retained. Fortunately, there is little spectral energy contained beyond 2 Hz (Figure 4b).

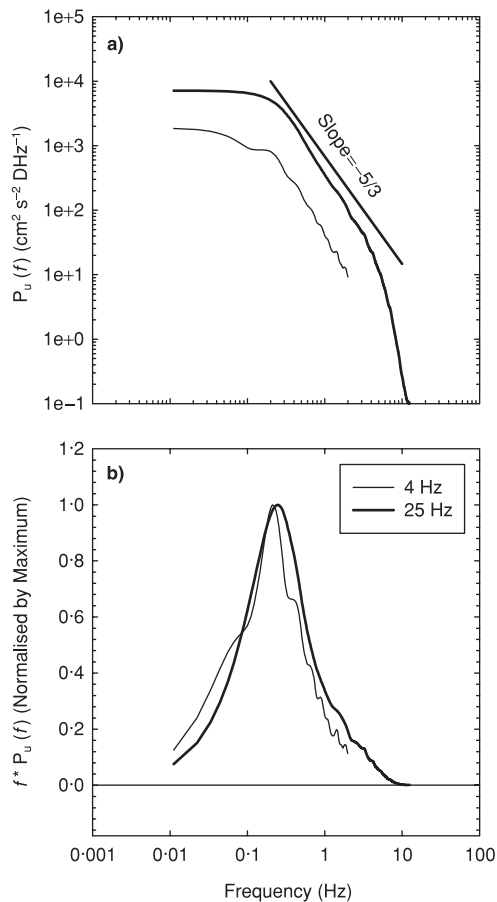


Figure 4. Streamwise component velocity spectra of File C calculated using data sampled at 25 Hz (the sampling rate used in the field) and data at 4 Hz (filtered and subsampled from the 25 Hz data). Spectra are plotted using two different plotting conventions: (a) conventional log–log plot that highlights spectral roll off, and (b) variance preserving form.

Table II. Velocity moments for field data files collected, calculated over 17-min periods. See Figure 5 for locations of files with respect to dune position

Moments	A	B	C	D	E	F	G	H	I	J	K
U (m s^{-1})	0.67	0.68	0.65	0.65	0.72	0.74	0.69	0.74	0.74	0.65	0.69
V (m s^{-1})	-0.04	-0.05	0.03	0.00	0.06	0.03	0.04	-0.02	-0.00	-0.02	-0.01
W (m s^{-1})	-0.04	-0.07	-0.10	-0.09	-0.14	-0.13	-0.13	-0.12	-0.06	-0.04	-0.04
Rms u (m s^{-1})	0.14	0.13	0.15	0.18	0.12	0.11	0.10	0.10	0.09	0.10	0.10
Rms v (m s^{-1})	0.08	0.07	0.09	0.08	0.08	0.07	0.07	0.07	0.07	0.08	0.05
Rms w (m s^{-1})	0.07	0.07	0.09	0.08	0.06	0.05	0.06	0.05	0.04	0.06	0.05
θ (degrees)	7.29	6.17	12.76	10.37	15.17	13.20	13.99	8.68	9.94	8.33	9.52
F_{err} (%)	-1.95	-0.76	-2.75	-2.34	-3.06	-1.76	-1.60	-1.34	-1.94	-6.08	-3.53

Further, in the frequency range under examination (that bearing coherent flow structures), the velocity spectra based on 25 Hz and 4 Hz sampling rates have the same shape. If the data were only decimated, the noise would be retained in the signal. If the data were only filtered, information on higher frequency motions (smaller scale eddies), which did not agree with the standard model, would have been retained in the velocity signal.

Since the ADV was mounted on a fixed frame, the measurement volume was positioned at varying heights above the bottom as the dune migrated past the array (0.42 m, 0.09 m, and 0.04 m above the dune trough, stoss slope, and crest, respectively). Prior to deployment of the fully assembled frame, care was taken to ensure that the ADV was aligned orthogonal to the frame axes so that spanwise (cross-stream) velocity would be measured laterally along the frame axis and vertical velocity would be measured along the vertical plane of the frame. During deployment, the instrument frame was oriented visually according to the mean surface flow lines. Despite careful attention to alignment, the recorded velocity signals indicate that the sensor was slightly misaligned relative to flow at depth (i.e. the mean spanwise vector was not zero). The near-bottom flow direction deviated slightly from the surface flow line, likely because of the presence of large bedforms. Indeed, the flow field beneath the probe shifted progressively throughout the measurement period because of dune migration and evolution. The velocity components were rotated orthogonally to compensate for this.

The horizontal velocity components were rotated according to the following convention

$$\begin{aligned} u_r &= u_m \cos \theta + v_m \sin \theta \\ v_r &= -u_m \sin \theta + v_m \cos \theta \end{aligned} \quad (1)$$

where subscripts m and r refer to the measured and rotated velocity frames, respectively, and θ is the angle of 'misalignment' (e.g. Kaimal and Haugen, 1969). The rotation angle necessary to reduce the mean spanwise velocity to zero ranged from 6.17° to 15.16° (Table II) with a mean misalignment angle of 10.49° averaged over the entire 5.5 h period (eleven data files). Velocities were corrected using only the mean angle. By doing so, short-term variations in v caused by bedform migration and morphologic change are accepted as real.

Orthogonal rotation to reduce the mean vertical velocity to zero is often desirable (Roy *et al.*, 1996). The necessary rotation angles for this study varied from -3.14° to -10.73° with a mean of -7.03° . The flow field over a dune is expected to be complex and it is not unreasonable to expect mean vertical currents over large bedforms at near-bottom locations. Careful preparatory work before and during sensor deployment suggests that the sensor was truly aligned in the vertical and that there was no contamination of the horizontal flow component. Thus, no correction was applied, and mean vertical currents were accepted as real.

Fractional error of the measured Reynolds stress, F_{err} , resulting from the spanwise misalignment was calculated as

$$F_{err} = \frac{\overline{u'_m w'_m} - \overline{u'_r w'_m}}{\overline{u'_r w'_m}} \quad (2)$$

where u' and w' are fluctuations about the mean (Kaimal and Haugen, 1969). Table II shows F_{err} ranges from 0.11–0.73 per cent per degree. These values represent the error due to: (1) misalignment of each individual file and, (2) the mean bias over the measurement period caused by accepting short-term deviations from the mean streamlines as real.

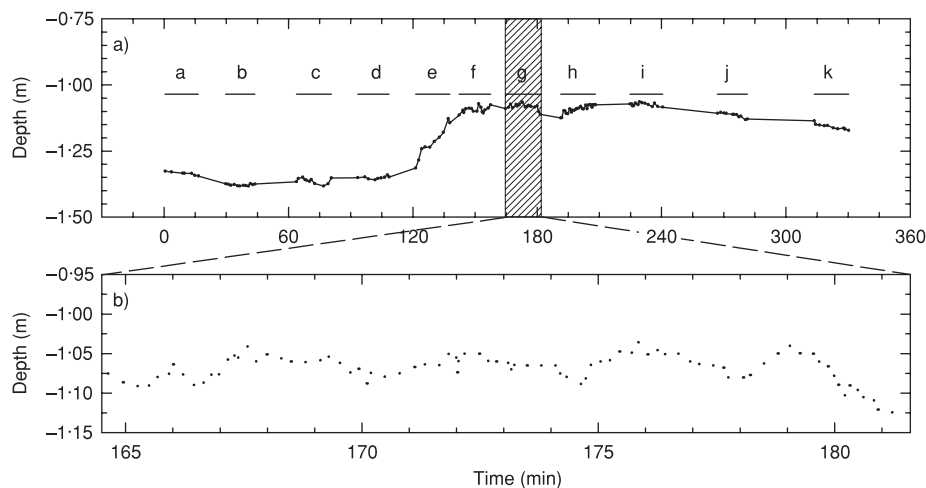


Figure 5. (a) Dune geometry. (b) Secondary bedforms on stoss slope of dune. Horizontal marking lines are at the elevation of the ADV sampling volume.

Time-averaged Flow Conditions

The dune profile derived from the echo sounder measurements is shown in Figure 5a. Since the instrument frame was fixed to the bed and the dune migrated past the frame, dune geometry in Figure 5a is presented as a function of time rather than horizontal distance. Mean flow depth, d , across the dune was 1.18 m with maximum flow depth, d_{\max} , over the trough of 1.38 m and minimum flow depth, d_{\min} , over the crest of 1.06 m. Dune height was 0.32 m with a height to depth ratio $H/d = 0.27$. The nearest upstream dune, measured using a stadia rod, had a height of $c. 0.35$ m. Dune wavelength was estimated to be $c. 4.5$ m, which is consistent with the range of wavelengths measured for dozens of other dunes in the study reach (Table I). The corresponding dune steepness was therefore $H/\lambda = 0.07$ and the mean migration rate (based on estimated λ and the echo sounder profile) was approximately 0.36 m h^{-1} . The stoss side of the dune appears to be rippled with secondary bedforms having heights of approximately 0.05 m (Figure 5b).

The lower portions of the boundary layer structure can be inferred from its geometry in relation to the geometry of the bedform. This provides a rough estimate of where the probe is in terms of the turbulent flow structure described in the introduction. Based on laboratory experiments (e.g. McLean, 1990; Nelson *et al.*, 1993; McLean *et al.*, 1994; Bennett and Best, 1995; Venditti and Bennett, 2000), the wake region typically begins at the bedform crest and extends downstream over the next crest. Its thickness grows with distance from the crest, but is typically $1-2H$ at its maximum thickness. Over this dune the wake structure should be $c. 0.3-0.6$ m in thickness. The flow separation cell extends $5H$ downstream of the crest, or $c. 1.6$ m over this dune. The IBL typically grows with distance downstream of the flow separation cell and, when fully developed, has a thickness of $0.25H$ or 0.08 m over this dune. Based on this geometry of the flow, Files A–D should be in the wake, File E is over the separation cell and shear layer, F–J are in the IBL and K is in the lower portion of the dissipating wake. These designations are given in Figure 6e.

The mean (U , V , W) and root-mean-square velocity (rms u , rms v , rms w) moments for individual data files are presented in Table II. Averages over 3-min sections of the individual files showed no within-time-series trends, so averages represent the full 17-min time series. The mean streamwise velocity, \bar{U} , of all eleven measurement files was 0.69 m s^{-1} . The flow responds to the bed topography in that it is accelerated over the dune crest and decelerated over the dune trough. Over the crest \bar{U} is 0.73 m s^{-1} while over the stoss slope and trough \bar{U} is 0.70 and 0.66 m s^{-1} , respectively. The larger survey of the entire reach using depth-integration techniques showed that the mean flow velocity over bedform crests in this area of the dune field was $c. 0.65-0.75 \text{ m s}^{-1}$. Some flow acceleration is expected over the dune crest, so $\bar{U} = 0.69 \text{ m s}^{-1}$ seems to be a fairly representative mean velocity over this dune near the bed.

Several commonly reported turbulence parameters are plotted in Figure 6 with respect to horizontal position along the dune profile including (i) turbulence intensities (I_u , I_v , I_w) calculated using

$$I_u = \frac{\text{rms } u}{U}, \quad I_v = \frac{\text{rms } v}{U}, \quad I_w = \frac{\text{rms } w}{U} \quad (3)$$

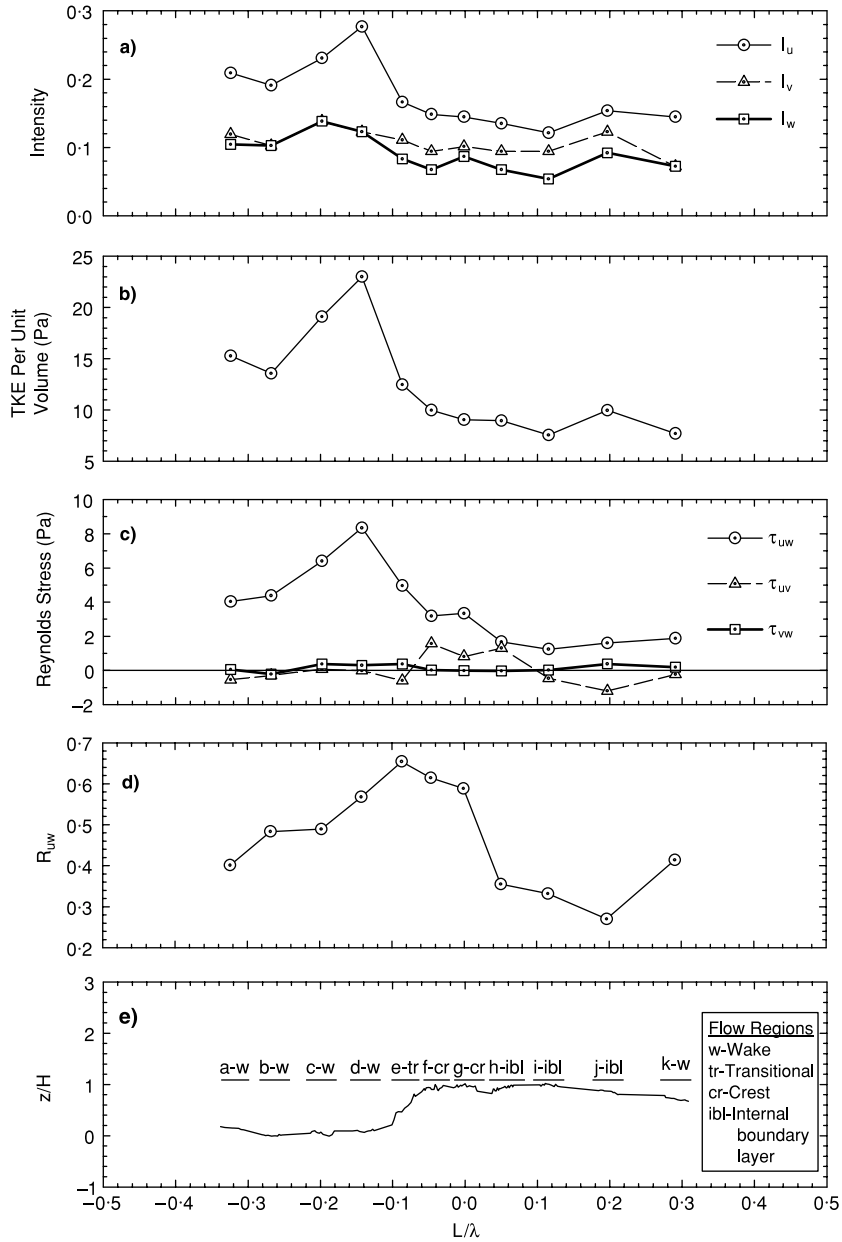


Figure 6. Time-averaged turbulence quantities over the dune: (a) turbulent intensity; (b) TKE; (c) Reynolds stresses; and (d) boundary layer correlation coefficient, R_{uw} . (e) Trace of the dune with interpretation of the structural components of flow at each measurement location. Height of bed above datum, z , is normalized by dune height, H . All panels are plotted such that distance along the dune, L , is normalized by bedform wavelength, λ . $L/\lambda = 0$ approximately conforms to the location of maximum elevation. The transition from the lee side of the dune to the stoss side occurs at $L/\lambda \approx -0.08$.

(ii) turbulent kinetic energy per unit volume (TKE) estimated using

$$TKE = \frac{1}{2} \rho (\overline{u'^2} + \overline{v'^2} + \overline{w'^2}) \tag{4}$$

where $u' = u - U$, $v' = v - V$, and $w' = w - W$, (iii) the Reynolds shear stresses (τ_{uw} , τ_{uv} , τ_{vw}) calculated using

$$\tau_{uw} = -\rho \overline{u'w'}, \quad \tau_{uv} = -\rho \overline{u'v'}, \quad \tau_{vw} = -\rho \overline{v'w'} \quad (5)$$

and (iv) the boundary-layer correlation coefficient, R_{uw} , given by

$$R_{uw} = \frac{-\overline{u'w'}}{\text{rms } u \cdot \text{rms } w} \quad (6)$$

Dune topography (Figure 6e) is presented in dimensionless form with λ and H as normalizing variables.

Laboratory measurements (Bennett and Best, 1995; Venditti and Bennett, 2000) suggest that $I_u = 0-0.2$ over most of the dune with nominally larger values in the wake ($I_u = 0.2-0.4$) and much larger values ($I_u \gg 0.4$) at the reattachment point and in the separation cell. Figure 6a shows that I_u values above the trough range between 0.20 to 0.25. As the bedform migrates below the sensor, I_u initially rises to a maximum of 0.28 immediately downstream of the dune brink, then is reduced (<0.2) over the bedform crest and stoss slope. Similar spatial trends characterize I_v and I_w , although $I_v \approx I_w \approx 0.5I_u$.

TKE represents the energy extracted from the mean flow by the motion of turbulent eddies (Kline *et al.*, 1967; Bradshaw, 1977). TKE production involves interactions of the Reynolds stresses with mean velocity gradients and, ultimately, TKE dissipation occurs via viscous forces after being passed through the inertial subrange of the turbulence spectrum (Tennekes and Lumley, 1972). Venditti and Bennett (2000) demonstrated that TKE production is most prominent in the separation cell and at the reattachment point. Elevated values also occur in the wake region. Figure 6b shows that TKE production (eddy generation) is largest (23 Pa) a short distance downstream of the dune brink where the shear layer should be most pronounced. Minimum observed TKE values of 6–10 Pa are found over the crest and stoss slope.

Typically, the τ_{uw} component of the Reynolds shear stress is largest in the separation cell and elevated values occur in the wake region. The rest of the flow field is characterized by relatively smaller τ_{uw} values (Nelson *et al.*, 1993; McLean *et al.*, 1994; Bennett and Best, 1995; Venditti and Bennett, 2000). It is important to distinguish this shear stress distribution along a horizontal plane from the boundary shear stress distribution along the bedform surface, which typically reaches a maximum a short distance upstream of the dune crest (Nelson *et al.*, 1993; McLean *et al.*, 1994). The local boundary shear stress could not be calculated because the instruments were mounted on a fixed frame at a fixed depth.

The observed Reynolds stresses are greatest in the lee of the dune and smallest over the stoss slope, as was the case for turbulence intensity and TKE. It is clear that τ_{uw} dominates the momentum-exchange process over the entire dune profile and, as expected, the bulk of the momentum transfer is directed toward the bed ($\tau_{uw} > 0$). Negligible contributions to the overall momentum balance come from τ_{uv} and τ_{vw} and relatively little momentum exchange occurs laterally. However, τ_{uv} shifts progressively from making small positive contributions over the crest to small negative contributions over the stoss slope. This may be due to the migrating dune forcing slight deviations in the mean orientation of the near-bottom flow lines.

The boundary-layer correlation coefficient ($-1 \leq R_{uw} \leq 1$) is a normalized covariance that expresses the degree of linear correlation between u and w velocity fluctuations. As such, R_{uw} is a 'local' statistic that provides insight into the presence or absence of flow structure at a specific location. In flow over a flat bed, there is little streamwise variation in R_{uw} and values of $c. 0.5$ are typical of the near-bed regions while decreased values of 0.0–0.3 are found in the outer flow region (Nezu and Nakagawa, 1993). For flow over laboratory dunes, Nelson *et al.* (1993) and Venditti and Bennett (2000) suggest that $R_{uw} < 0.3$ within the IBL, $R_{uw} \approx 0.3-0.5$ in the outer flow region, and $R_{uw} > 0.6$ in the wake and in the separation cell. Over the field dune, values of R_{uw} are in the range 0.25–0.65 (Figure 6d), which is consistent with other studies. The smallest correlation occurs across the stoss slope, presumably in association with the IBL, and the largest correlation was found in the wake region. The maximum observed R_{uw} occurs immediately downstream of the dune brink, indicating u and w velocity fluctuations are strongly coupled through time as might be expected along a developing shear layer.

Given the elevated values of turbulence intensities, TKE, τ_{uw} and R_{uw} , the idea that Files A, B, C and D were collected in the wake seems reasonable. The turbulence statistics reveal that the File E was taken in a zone that is transitional between the highly turbulent wake and relatively well structured flow over the crest. This would be typical of flow above the separation cell.

Absolute values of I_u observed over the dune crest and stoss slope and values of R_{uw} at File H–J are comparable to those observed in the IBL in laboratory studies (see Nelson *et al.*, 1993; Bennett and Best, 1995; and Venditti and Bennett, 2000). Relatively smaller values of TKE and τ_{uw} confirm that Files F–J were collected in the IBL. The similarity between turbulence statistics values at Files H–J and File K suggests that the sensor was also in the IBL during its collection. This promotes the idea that the IBL over this dune is thicker than has been observed in laboratory

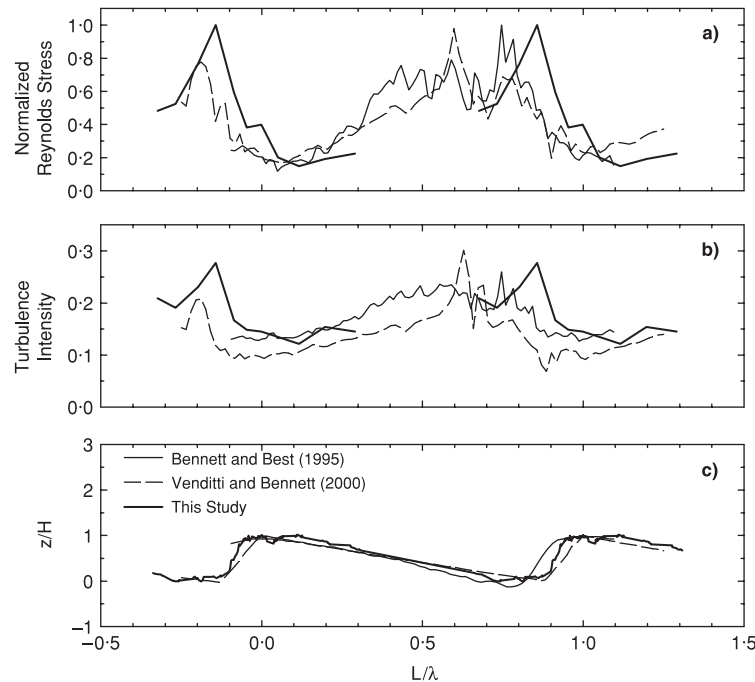


Figure 7. Comparison of (a) Reynolds stress, τ_{nor} , and (b) turbulence intensity, I_u , along horizontal transects over dune crests in this experiment and the laboratory experiments of Bennett and Best (1995) and Venditti and Bennett (2000). τ_{nor} is the observed Reynolds stress normalized by the maximum observed along the transect. (c) Trace of the dune, included for reference purposes. Height of bed above datum, z , is normalized by dune height, H . All panels are plotted such that distance along the dune, L , is normalized by bedform wavelength, λ . $L/\lambda = 0$ roughly conforms to the location of the dune crest. The transition from the lee side of the dune to the stoss side occurs at $L/\lambda \approx -0.08$.

research. Large R_{uw} values above the dune crest (Files F and G) and immediately in the lee (File E) are curious. At similar locations over a laboratory dune, Venditti and Bennett (2000) observed R_{uw} values of 0.25–0.45. These large R_{uw} values are similar to separation cell values observed in laboratory models. These elevated values are likely related to minor bedforms that migrated over the stoss slope of the field dune. Flows at Files F and G are given the designation ‘crest’ in Figure 6e to separate them from the IBL over the rest of the stoss slope.

There is a strong correlation between the pattern in turbulence parameters observed over dunes in the laboratory and our field results. Horizontal transects at the same relative depth as the field data were extracted from data presented by Bennett and Best (1995) and Venditti and Bennett (2000). Figure 7 presents the Reynolds stress normalized by the maximum observed along the transect, τ_{nor} , and I_u for all three studies. The field data do not cover an entire dune wavelength so they are displayed twice (at either end of the plot), whereas the laboratory data are continuous across two subsequent dune crests. Nearly identical trends in τ_{nor} and I_u are evident (Figure 7a and b) for the three studies, with elevated values in the lee of the crest and reduced values above the stoss slope of the dune. This supports the idea that the field data conform to the conceptual model presented in Figure 1.

Coherent Flow Structures

Spectral and cospectral analysis

Previous research in the laboratory (Müller and Gyr, 1986; Bennett and Best, 1995; Venditti and Bennett, 2000) and in the field (Kostaschuk and Church, 1993; Kostaschuk, 2000) indicates that flow in the lee of a bedform is dominated by eddy-like motions. Although the exact nature of these eddies is not well understood it would appear that they are generated as a result of instabilities along a shear layer at the interface between the streaming flow over the crest and the slowly recirculating fluid in the separation cell underneath. A Kelvin–Helmholtz mechanism is often invoked for

the instability (e.g. Müller and Gyr, 1986) but, regardless of the exact dynamics, such fluid oscillations should have recognizable spectral signatures in frequency space. These spectral signatures should evolve spatially because instabilities along the shear layer are expected to lead to enhanced wave-like perturbations that may 'break' or 'roll up' into vortices that amalgamate, grow in size, and eventually diffuse as they are advected downstream (see Ho and Heurre, 1984; Müller and Gyr, 1986).

Spectral and cospectral analyses were performed on the velocity time series to search for recurring periodic motions in the flow field. Local non-stationarity in long velocity time series can introduce significant uncertainty into the velocity component spectra or cospectra. Changes in the frequency of turbulent events through time can produce bizarre and statistically insignificant results. Thus, it is necessary to conduct spectral analysis on portions of time series that are long enough to capture many cycles of the phenomena of interest while limiting possible contamination by non-stationarity. Thus, each 17-min file was broken into 3-min sections that were detrended and analysed separately. A rough estimate of the expected recurrence of turbulent events in the boundary layer over a dune can be made from scaling relations provided by Simpson (1989). These relations suggest that vortex shedding should occur at *c.* 2.3 s and wake flapping should occur at *c.* 19 s. Thus, the 3-min sections should be capable of capturing these turbulent events.

Energy density estimates were smoothed using a bandwidth of 0.2278 Hz, yielding approximately 55 degrees of freedom on the spectral estimates. The five resultant spectra for each data file were then averaged to produce the spectra shown in Figure 8. Spectra are plotted in variance-preserving form where energy density ($\text{cm}^2 \text{s}^{-2} \Delta \text{Hz}^{-1}$) is multiplied by frequency, f , so that the relative contribution to the total variance from a specific frequency band ($f, f + \Delta f$) is easily discerned (see Panofsky and Dutton, 1984; Kaimal and Finnegan, 1994). Upper and lower 95 per cent confidence intervals around the averaged spectra, calculated following the methods outlined in Jenkins and Watts (1968), are $1.1574 fP(f)$ and $0.8739 fP(f)$, respectively. Many researchers interpret spectral energy peaks in the context of eddy-like flow structures (e.g. Boppe and Neu, 1995), but Tennekes and Lumley (1972, p. 259) note that, even though a single wave-like oscillation may be legitimately associated with a single Fourier frequency, an eddy is associated with many Fourier coefficients and the phase relations among them. This implies that more sophisticated analyses are necessary to decompose a velocity field into eddies. Nevertheless, prominent eddies will still manifest themselves as broad spectral peaks within a spectrum.

Cospectral analysis was conducted on the joint u and w time series following the same conventions as for the individual velocity components, and these results are also plotted in Figure 8. In a one-dimensional velocity spectrum (e.g. u or w), the variance is proportional to the Reynolds normal stress (i.e. $\overline{u'^2}$ or $\overline{w'^2}$), whereas in a cross-spectrum, the covariance between two velocity components is proportional to the Reynolds shear stress ($\overline{u'w'}$). The coherency-squared spectrum is interpreted as a frequency-specific correlation coefficient (Jenkins and Watts, 1968), and it shows the significance of the cross-spectral estimate at a specific frequency band. The coherency-squared spectrum of isotropic turbulence should be 'white' because of the absence of correlation or ordered structure in the flow. In shear flows or a boundary layer, u and w velocity fluctuations are partly correlated, and the coherency squared spectrum should display peaks and valleys accordingly.

The spectra presented in Figure 8 show that spectral energy varies in response to changing signal variance and is about two to four times greater in the lee of the dune (Files A, B, C, D) than over the crest (Files F, G). The smallest spectral energies are found over the stoss slope (Files H, I, J, K). Streamwise velocities have peak variances at frequencies between 0.17 and 0.29 Hz with a mean around 0.22 Hz (4.5 s). Spectra for v and w contain peaks at higher frequencies with means of 0.56 Hz (1.8 s) and 0.44 Hz (2.3 s) respectively. The cross-spectra tend to have peaks at slightly higher frequencies than the corresponding u spectra, which is not surprising given that high frequency information in the w time series is captured in a joint cross-spectrum.

Over the stoss slope of the dune, spectra and cross-spectra show minimal frequency structure as well as greatly reduced spectral and cospectral energy. This is similar to observations by Venditti and Bennett (2000) for spectra in the IBL in their flume experiments. Streamwise spectra are flat without discernible peaks, and w spectral variance is relatively large as compared to u . Peaks and valleys in the coherency-squared spectra and cross-spectra suggest that velocity fluctuations are weakly correlated and without dominant frequencies. These weak hydrodynamic signatures are interpreted as 'relict' motions that are imposed on the IBL from above (e.g. Müller and Gyr, 1986; Venditti and Bennett, 2000). Coherency-squared spectra at File H suggest this measurement is transitional between the stoss and crest areas of the dune.

Over the dune crest (Files F and G), the velocity spectra and cross-spectra are also subdued and relatively featureless suggesting the absence of recurring oscillatory motions at dominant frequencies. Close to the dune brink (File F), there is evidence of an emerging u spectral peak centred at *c.* 0.2 Hz. The peaks in w have shifted to a lower frequency. Coherency-squared spectra for Files F and G display large and well-defined peaks at about 0.1 Hz. This suggests that flow over the crest is becoming structured and that the u and w motions are becoming coupled in frequency space. File

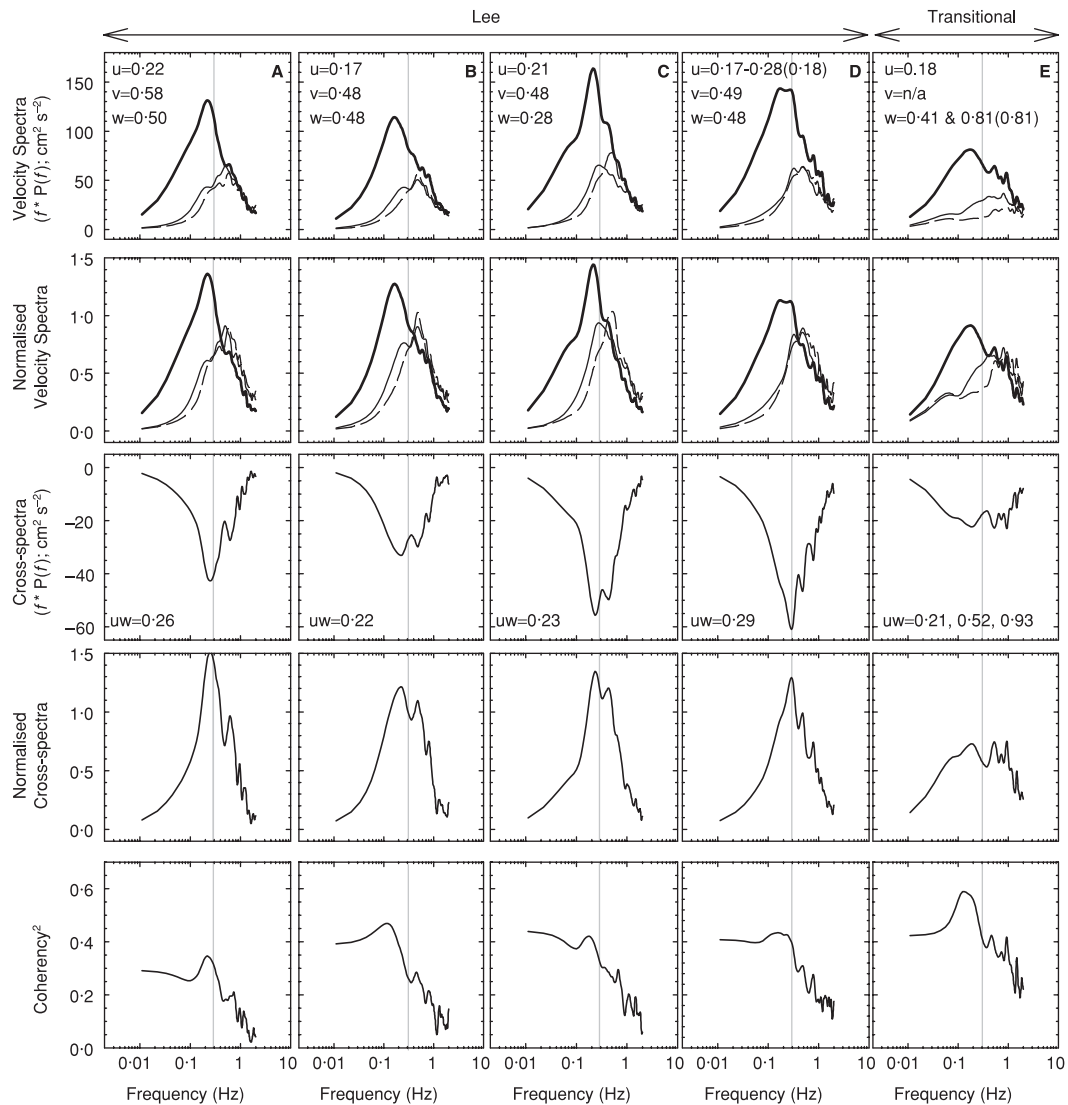


Figure 8. Turbulence spectra (upper two rows of panels), cross-spectra (middle two rows of panels), and coherency-squared spectra (bottom panels) for files along the horizontal transect over the dune. Spectra (cospectra) are normalized by the total spectral variance (covariance). Non-normalized spectra provide information on the relative signal variance. Normalized spectra eliminate the effects of signal variance and allow comparisons of the spectral shapes and peak frequencies. Letters A–K indicate files displayed in each panel. If there is a discernible peak in the spectrum, the frequency corresponding to the maximum spectral energy is reported. Where the spectrum appears to peak over a wide range of frequencies, the range is reported with the maximum in brackets. In some cases, no discernible peak could be identified (reported as n/a).

E, taken in the transitional zone, is at the onset of the shear layer instability. Spectral energy values increase, and even though there is as yet no dominant spectral peak, there is a prominent peak in the coherency-squared spectrum.

Farther downstream in the lee of the dune crest (Files A–D), there is much greater variance (covariance) in the spectra (cross-spectra) and the frequency structure becomes more sharply defined with single, dominant peaks. Coherency-squared spectra show strong correlations across the low frequency domain with notable decay at frequencies greater than 0.3 Hz. In contrast to the stoss slope, coherency spectra in the lee of the dune have a dominant or preferred peak. This overall pattern of flow signatures is consistent with flow over rearward-facing steps (see Simpson, 1989, figures 6 and 7).

It is interesting to note that in the transition between the crest and the lee (i.e. at File E), the spectral peaks in v and w are shifted to higher frequencies than in the u spectrum. This shift persists downstream in the wake zone. Venditti

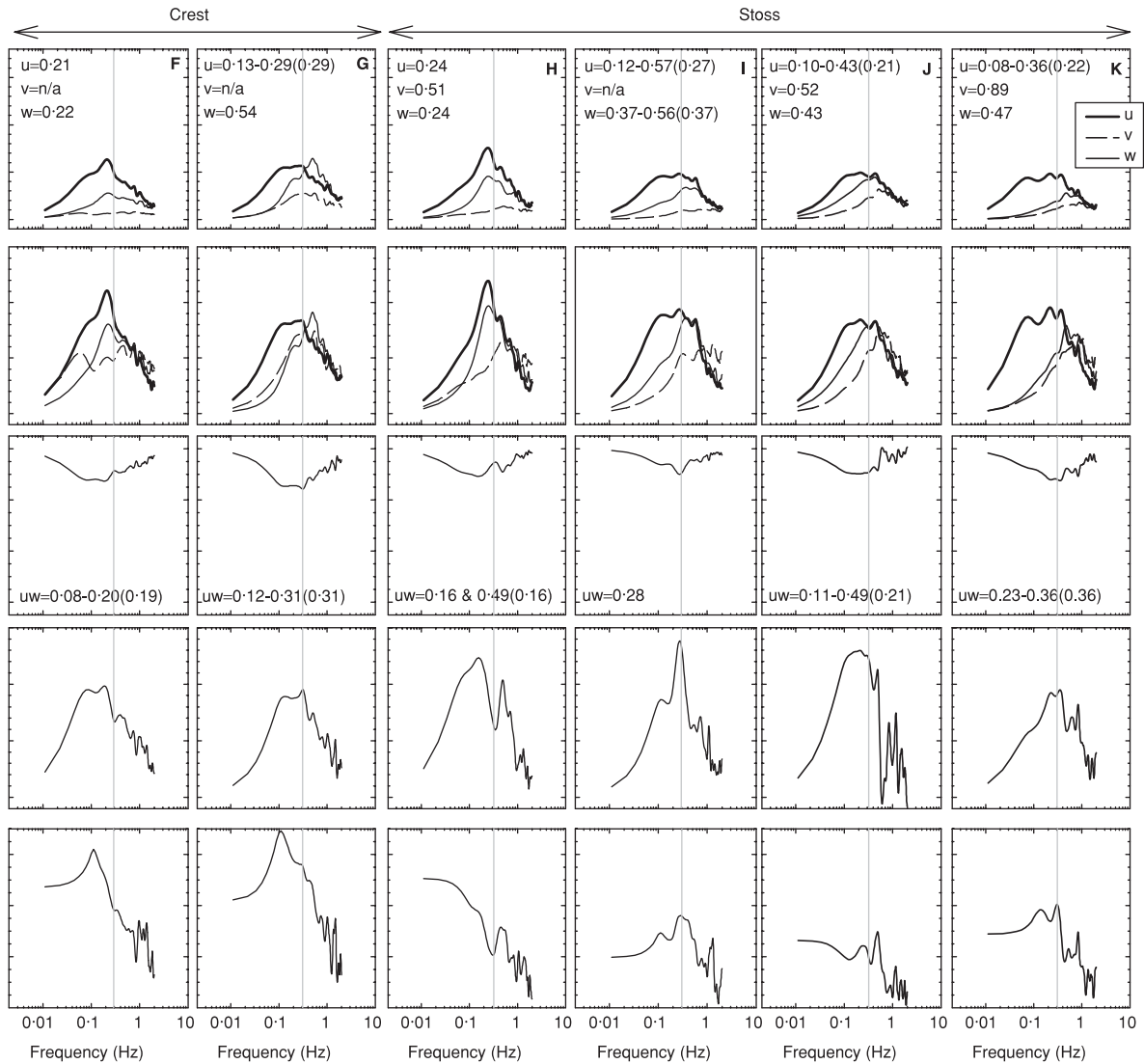


Figure 8. (continued)

and Bennett (2000) suggested that this shift is due to eddy stretching and elongation by the mean flow, but it may also indicate that there are two significant scales of oscillation in the flow system. The high frequency oscillations in the w spectra may be associated with fine-scale waves and micro-vortices generated in the classic sense of a shear layer instability. The lower frequency oscillations that dominate the u velocity fluctuations near File E and downstream are likely associated with the onset of coarse-scale undulations in the shear layer leading to wave breaking and eddy shedding. Müller and Gyr (1986) suggest that vortex growth and Kelvin–Helmholtz instability-induced wave breaking should reach a maximum intensity at a downstream distance of approximately $1.5H$ from the dune crest (corresponding roughly to File D), which is precisely where single dominant frequency peaks begin to appear in the spectra. There is no evidence in support of the wake ‘flapping’ described by Simpson (1989) and discussed in Nelson *et al.* (1993) and Kostaschuk (2000). However, none of the measurements are from the separation zone so the spectra may not reflect this process. Further, if these events are only occurring intermittently, then splitting the time series and averaging the spectra and cospectra may prevent their observation.

At Files A and B, total spectral energy has decreased and the spectral peaks are not as pronounced, suggesting that the primary vortices are indeed beginning to diffuse and dissipate. Tennekes and Lumley (1972) suggest that eddies lose their identity because of interactions with other eddies that occur within one or two periods or wavelengths.

Strouhal similarity

Absolute time and length scales vary amongst river channels and are considerably larger than those in laboratory channels. It is of interest, therefore, to determine whether the quasi-periodic flow structures evident in the lee of the Green River dunes are geometrically and kinematically similar to laboratory and other field dunes when scaled appropriately. The Strouhal number is a non-dimensional frequency of the following form

$$Sr = \frac{fl}{U} \quad (7)$$

where l and U are characteristic length and velocity scales, and f is the frequency of oscillation (Rouse, 1946). Some confusion persists in the literature regarding the application of Sr to fluvial systems largely because there are several candidates for a characteristic length scale (e.g. boundary layer thickness, d , H , X_R) and for a characteristic velocity scale (free-stream velocity, depth-averaged velocity, u_s). The length and velocity scales must be commensurate with the process Sr is to characterize. Further complicating this issue is that variants of Sr have been proposed (e.g. its reciprocal, which yields mean period or recurrence interval) without reference or conversion to Sr (e.g. Rao *et al.*, 1971) thereby giving the impression that there are several different non-dimensional predictors of eddy-shedding frequency. The confusion is exacerbated when an approximate numerical value for Sr is calculated for a well-defined system (e.g. a quartz sphere settling at low Re through a still fluid) and later adopted as a universal constant for the purposes of predicting the period of oscillation for another unrelated system (e.g. vortex shedding in the lee of a dune at large Re). Kostaschuk and Church (1993) discuss this issue and note that in one formulation the constant $1/Sr$ is equal to 2π , whereas in another it adopts a value of 3–7 with a mean of 6. Rouse (1946, p. 241), in discussing wakes behind cylinders, shows that there is a strong Reynolds number dependency for this parameter, and that a value of 5 holds for $2 \times 10^2 < Re < 2 \times 10^5$, but the value decreases to about 2.5 beyond this range.

Despite the broad range of possible values for Sr there is, in fact, some consistency in fluvial systems when similar conventions are employed. Table III shows the results reported in several studies of flow over dunes using mean velocity as the velocity scale and d or versus H as the length scale. The data in Table III are from studies that used either flow visualization techniques or spectral analysis to determine eddy frequencies in fully turbulent flow. The data are further constrained to observations from the lee of bedforms. With few exceptions, reported values of Sr (when d is used) are in the range $0.3 < Sr(d) < 0.6$ (i.e. non-dimensional periods of about 2–3), whereas when H is used, $0.1 < Sr(H) < 0.25$ (i.e. non-dimensional periods of about 4–10). For the Green River data, $Sr(d) \approx 0.29$ – 0.46 and $Sr(H) \approx 0.10$ – 0.13 . Some of these values are at the low end of the expected range, but the general agreement is good.

Table III. Strouhal numbers for field and laboratory studies using spectral analysis of time series or flow visualization techniques to determine eddy periods in the lee of bedforms

Author	Measurement	T(s)	d(m)	U(m s ⁻¹)	H(m)	Sr(d)	Sr(H)
<i>Field studies</i>							
This study	ADV-u	4.54	1.18	0.69	0.32	0.38	0.10
	ADV-uw	2.94				0.58	0.16
Kostaschuk and Church (1993)	Acoustic soundings*	33	1.1	0.72§	2.2	0.46	0.09
		66				0.23	0.05
Kostaschuk (2000)	ECM-u	128:00	9.1	0.38	2.92	0.19	0.06
		85:32				0.28	0.09
<i>Laboratory studies</i>							
Venditti and Bennett (2000)	ADV-u	0.82	0.175	0.46	0.04	0.47	0.11
	OBS-c†	0.74				0.52	0.12
Müller and Gyr (1986)	FV	~1	0.16	0.40	0.10	0.4	0.25
Ikeda and Asaeda (1993)	HWA	n/a	n/a	n/a	n/a	0.35–0.42	n/a
Itakura and Kishi (1980)	FV	2.92	0.064	0.31	0.15	0.60	0.14
Nezu <i>et al.</i> (1980)	FV	n/a	n/a	n/a	n/a	0.33–0.50	n/a

ECM, electromagnetic current meter; FV, flow visualization; OBS, optical backscatter probe; HWA, hot wire anemometer.

* Based on sediment plume periods.

† Based on sediment concentration time series.

§ Free stream velocity.

If only the data in the lee of the dune (Files A–E) are considered, the average $Sr(H) \approx 0.09$ and the average $Sr(d) \approx 0.33$, which translates into a mean recurrence period of 5.1 s for eddy-shedding from the dune crest. A simple visual count of surface boils moving past the instrument frame yielded 20 events over a 112 s interval, giving a recurrence period of 5.6 s. Surface boils occurred in intermittent groups with intervening periods when no boils appeared at the surface. Given that these boils were generated upstream of the study dune and that all shed eddies are not expected to produce surface boils, the agreement is intriguing.

Summary and Conclusions

Aspects of turbulent flow over a dune in a river channel are examined using detailed echo-sounder and acoustic Doppler velocimeter measurements. Based on the geometric position of the velocity sensor over the bedforms, measurements were taken in the wake, in transitional flow at the bedform crest, and in the internal boundary layer. The time-averaged turbulent flow field above a dune in a river channel is qualitatively consistent with a conceptual model that derives from flume studies. Furthermore, the data correspond quite well with published laboratory data (e.g. Nelson *et al.*, 1993; Bennett and Best, 1995; Venditti and Bennett, 2000). Measurements in the lee of the bedform are in the wake where large turbulent intensities, TKE, and turbulent shear stresses occur. Measurements over the stoss slope and crest are in an internal boundary layer where values of these parameters are greatly reduced. The large R_{uv} values over the crest demonstrate the flow is well structured (u and w velocity fluctuations are strongly coupled through time). Regardless of location over the dune, $I_v \approx I_w \approx 0.5I_u$ and the τ_{uw} component of the Reynolds shear stress dominates the momentum exchange.

Peak and total spectral and cross-spectral energies vary along the transect in a manner consistent with the flow signatures of wave-like perturbations that ‘break’ or ‘roll up’ into vortices that amalgamate, grow in size, and eventually diffuse as they are advected downstream. Spectral energies are small over the stoss slope of the dune and there is no dominant or preferred eddy frequency. Over the dune crest this pattern persists, although coherency-squared spectra display large and well defined peaks indicating u and w motions are also strongly coupled in frequency space. Beyond the dune brink this pattern persists where flow separation begins and the shear layer begins to grow. Further downstream, in the lee of the bedform, where the shear layer becomes unstable, spectral energies grow and are confined to a more narrow peak than over the crest; however, coherency-squared spectral peaks become broader as u and w motions are not as strongly coupled as over the crest. Strouhal number calculations, using mean depth or dune height and mean velocity, reveal broad similarity amongst eddies produced over field and laboratory bedforms. Correspondence between intermittently produced surface boils and normalized spectral peaks is observed.

Acknowledgements

T. Trexler and M. Kammerer provided congenial field support. J. Schmidt is thanked for facilitating various opportunities and for his friendship and good humour when they were essential. Financial support to J.V. came through the University of Southern California, the University of British Columbia, and a NSERC Post-Graduate Scholarship. The project was partly funded through grants from the Geography and Regional Science Program (NSF) and the National Park Service. The manuscript has benefited from the constructive reviews of S. Bennett, M. Church, M. Hassan and two anonymous reviewers.

References

- Bennett SJ, Best JL. 1995. Mean flow and turbulence structure over fixed, two-dimensional dunes: implications for sediment transport and bedform stability. *Sedimentology* **42**: 491–513.
- Biron P, Roy AG, Best JL. 1995. A scheme for resampling, filtering, and subsampling unevenly spaced laser Doppler anemometer data. *Mathematical Geology* **27**: 731–748.
- Boppe RS, Neu WL. 1995. Quasi-coherent structures in the marine atmospheric boundary layer. *Journal of Geophysical Research* **100**: 20635–20648.
- Bradshaw P. 1977. *An Introduction to Turbulence and its Measurement*. Pergamon Press: New York.
- Engel P. 1981. Length of flow separation over dunes. *Journal of the Hydraulic Division of American Society of Civil Engineers* **107**: 1133–1143.
- Ho C-M, Heurre P. 1984. Perturbed free shear layers. *Annual Review of Fluid Mechanics* **16**: 365–424.
- Ikeda S, Asaeda T. 1983. Sediment suspension with rippled bed. *Journal of Hydraulic Engineering* **109**: 409–423.
- Itakura T, Kishi T. 1980. Open channel flow with suspended sediments on sand waves. In *Proceedings of the Third International Symposium on Stochastic Hydraulics, Tokyo, Japan*, Kikkawa H, Iwasa Y (eds). International Association of Hydraulic Research: Tokyo, Japan; 589–598.

- Jackson RG. 1976. Sedimentological and fluid-dynamic implications of the turbulent bursting phenomenon in geophysical flows. *Journal of Fluid Mechanics* **77**: 531–560.
- Jenkins GM, Watts DG. 1968. *Spectral Analysis and Its Applications*. Holden-Day: San Francisco.
- Kaimal JC, Finnegan JJ. 1994. *Atmospheric Boundary Layer Flows: Their Structure and Measurement*. Oxford University Press: New York.
- Kaimal JC, Haugen DA. 1969. Some errors in the measurement of Reynolds stress. *Journal of Applied Meteorology* **8**: 460–462.
- Kline SJW, Reynolds WC, Schraub FA, Rundstadler PW. 1967. The structure of turbulent boundary layers. *Journal of Fluid Mechanics* **30**: 741–773.
- Kostaschuk RA. 2000. A field study of turbulence and sediment dynamics over subaqueous dunes with flow separation. *Sedimentology* **47**: 519–531.
- Kostaschuk RA, Church MA. 1993. Macroturbulence generated by dunes: Fraser River, Canada. *Sedimentary Geology* **85**: 25–37.
- Kostaschuk RA, Villard P. 1996. Flow and sediment transport over large subaqueous dunes: Fraser River, Canada. *Sedimentology* **43**: 849–863.
- Lohrmann A, Cabrera R, Kraus NC. 1994. Acoustic-Doppler Velocimeter (ADV) for laboratory use. *Proceedings of Fundamentals and Advancements in Hydraulic Measurements and Experimentation*. American Society of Civil Engineers: Buffalo, NY.
- Matthes GH. 1947. Macroturbulence in natural stream flow. *Transactions of the American Geophysical Union* **28**: 255–262.
- McLean SR. 1990. The stability of ripples and dunes. *Earth Science Reviews* **29**: 131–144.
- McLean SR, Nelson JM, Wolfe SR. 1994. Turbulence structure over two-dimensional bed forms: implications for sediment transport. *Journal of Geophysical Research* **99**: 12729–12747.
- McLean SR, Nelson JM, Shreve RL. 1996. Flow-sediment interactions in separating flows over bedforms. In *Coherent Flow Structures in Open Channels*, Ashworth PJ, Bennett SJ, Best JL, McLelland SJ (eds). John Wiley & Sons: Chichester; 203–226.
- Mesotech 1984. *Instrument Manual Model 807-12 (5M), Echo Sounder Module*. Mesotech: Port Coquitlam, British Columbia.
- Müller A, Gyr A. 1982. Visualization of the mixing layer behind dunes. In *Mechanics of Sediment Transport*, Sumner BM, Müller A (eds). A.A. Balkema: Rotterdam; 41–45.
- Müller A, Gyr A. 1986. On the vortex formation in the mixing layer behind dunes. *Journal of Hydraulic Research* **24**: 359–375.
- Nelson JM, McLean SR, Wolfe SR. 1993. Mean flow and turbulence fields over two-dimensional bed forms. *Water Resources Research* **29**: 3935–3953.
- Nezu I, Nakagawa H. 1993. *Turbulence in Open-Channel Flows*. A.A. Balkema: Rotterdam.
- Nezu I, Nakagawa H, Tominaga A, Yoshikawa M. 1980. Visual study of large-scale vortical motions in open-channel flow. *Annual Conference of the Japanese Society of Civil Engineers*. Japanese Society of Civil Engineers: Kansai-Branch, Japan; I1–I10 (in Japanese).
- Panofsky HA, Dutton JA. 1984. *Atmospheric Turbulence: Models and Methods for Engineering Applications*. Wiley: New York.
- Rao KN, Narashima R, Narayanan MAB. 1971. The ‘bursting’ phenomenon in a turbulent boundary layer. *Journal of Fluid Mechanics* **48**: 339–352.
- Rouse H. 1946. *Elementary Mechanics of Fluids*. Dover Publications: New York.
- Roy AG, Biron P, DeSerres B. 1996. On the necessity of applying a rotation to instantaneous velocity measurements in river flows. *Earth Surface Processes and Landforms* **21**: 817–827.
- Simpson RL. 1989. Turbulent boundary layer separation. *Annual Review of Fluid Mechanics* **21**: 205–234.
- Sontek. 1996. *ADV Operation Manual, Version 2.0*. Sontek: San Diego, California.
- Stone GW, Morgan JP. 1992. Jack-up pontoon barge for vibra-coring in shallow water. *Journal of Sedimentary Petrology* **62**: 739–741.
- Sukhodolov A, Thiele M, Bungartz H. 1998. Turbulence structure in a river reach with sand bed. *Water Resources Research* **34**: 1317–1334.
- Tennekes H, Lumley JL. 1972. *First Course in Turbulence*. MIT Press: Cambridge, Massachusetts.
- Venditti JG, Bennett SJ. 2000. Spectral analysis of turbulent flow and suspended sediment transport over fixed dunes. *Journal of Geophysical Research* **105**: 22035–22047.
- Yalin MS. 1992. *River Mechanics*. Pergamon Press: New York.